JOURNAL OF SOLID STATE CHEMISTRY 116, 300–306 (1995)

A New Ordered Oxygen-Deficient Perovskite $Sm_2Sr_6Cu_8O_{17+\delta}$: HREM Study of PLD Thin Films

B. Mercey,* A Gupta,† M. Hervieu,* and B. Raveau*

*Laboratoire CRISMAT, CNRS URA 1318 ISMRA, Université de Caen, Boulevard du Maréchal Juin, 14050 Caen Cedex, France; and †IBM Research Division, Thomas J. Watson Research Center, Yorktown Heights, New York 10598-0218

Received March 31, 1994; in revised form October 27, 1994; accepted October 31, 1994

A new ordered perovskite phase, $Sm_2Sr_6Cu_8O_{17+\delta}$, has been synthesized by reflection high-energy electron diffraction monitored pulsed laser deposition technique. It exhibits a supercell with $a \sim b \sim 2a_p\sqrt{2} = 10.89$ Å and $c = 3.66$ Å. A novel structure whose framework is built up from the intergrowth of $[CuO_2]_\infty$ and $[Cu_4O_9]_\infty$ chains running along $[010]_p$ and a Sm/Sr ordering is proposed from the electron microscopy observations. The analyses of the structure and the extended defects which arise in the matrix suggest that it should be possible to stabilize new intergrowths of $SrCuO_2$ and $SmSr_3Cu_4O_9$ structures.

INTRODUCTION

Besides its success in the growth of high quality thin films of high-T_c superconductors, the pulsed laser deposition (PLD) technique has also been gaining popularity as a synthetic tool for the preparation of new metastable phases. In particular, the epitaxial stabilization provided by the substrate can be exploited to enforce growth of phases which are thermodynamically unfavorable. For growth at low pressures, the ability to monitor and control the growth of layers using reflection high-energy electron diffraction (RHEED) is an additional attractive feature of the technique which can be utilized for the synthesis of new materials. In this perspective, the investigation of the *Ln*–Sr–Cu–O system is of interest since it offers the possibility of stabilizing novel oxygen-deficient perovskites which may be difficult or impossible to synthesize in the bulk; the formation of metastable phases with the substitution of rare earth for strontium in the infinite-layer structure is especially attractive.

Recently, the systematic investigation of the samarium-based system, of the formulation $Sm_{1-x}Sr_xCuO_{2.5+0.5x+\delta}$ corresponding to a perovskite, was carried out (1). It allowed a large homogeneity range of perovskite-type phases to be stabilized for $0.4 < x < 1$. A preliminary electron diffraction (ED) study showed the existence of extra spots and diffuse streaks in most of the ED patterns suggesting that complex ordering and nonstoichiometric phenomena are prevalent. In particular, for thin films corresponding to $x = 0.75$, a supercell was observed with "$2a_p\sqrt{2} \times 2a_p\sqrt{2} \times a_p$." This paper deals with the structural and microstructural characterization of thin films of a new ordered oxygen-deficient perovskite, $Sm_2Sr_6Cu_8O_{17+\delta}$ ($x = 0.75$).

FILM GROWTH AND EXPERIMENTAL: BRIEF RECALLS

The details for the RHEED-monitored pulsed laser deposition system have been described previously (2, 3). The films are grown using a KrF excimer laser ($\lambda = 248$ nm), at a low deposition rate (0.05–0.1 Å/pulse), with a pulse repetition frequency of 4 Hz and a fluence of 2–3 J/cm^2 at the target. The films are deposited on high-quality, optically polished (100)-oriented $SrTiO_3$ substrates. A high oxygen activity is provided during growth, while a low background pressure is maintained using a combination of atomic oxygen and pulsed molecular oxygen, as previously described (1).

The films have been deposited from one Sm/Cu/O target and one Sr/Cu/O target; the number of laser pulses on each target was calculated to obtain the desired theoretical composition. All the films, 500–700 Å thick, have grown at a substrate temperature of 600°C; following the deposition, the films were slowly cooled to room temperature after the chamber was backfilled with 760 Torr O_2.

The cation stoichiometry has been checked using EDAX and has been found to be within 5% of the expected values based on the programmed number of pulses used for ablation from each target. Standard four probe dc transport measurements have been used for electrical characterization of the films and have been described elsewhere (1). X-ray diffraction study was performed with a Siemens diffractometer in the normal Bragg reflection geometry. Transmission electron microscopy was carried out with a Philips EM420 (120 kV) electron microscope and high-resolution microscopy

0022-4596/95 $6.00

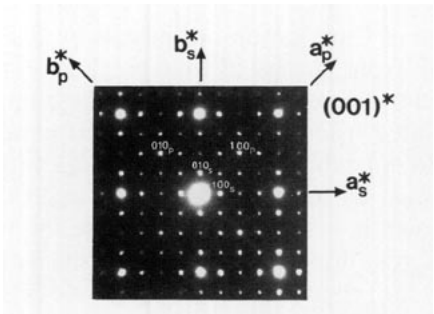

FIG. 1. [001] ED pattern; p refers to the perovskite subcell and s to the supercell with $a = 2a_p\sqrt{2}$.

(HREM) with a TOPCON 002B, having a resolution point of 1.8 Å.

RESULTS

The New Oxygen-Deficient Perovskite $Sm_2Sr_6Cu_8O_{17+\delta}$

For the molar ratio Sr/Sm = 3, the ED investigation of the thin films shows that most of the crystals exhibit a superstructure with respect to the "$a_p \times a_p \times c_p$" $SrCuO_2$ infinite layer structure. The examination of the films along the direction perpendicular to the substrate displays (001)* ED patterns (Fig. 1) with $a \approx b \approx 2\ a_p\sqrt{2}$. From the reconstruction of the reciprocal space, one observes that there are no conditions limiting the reflections and that the c parameter directed perpendicular to the substrate plane is close to that of the $SrCuO_2$ infinite layer structure. The c-axis value determined from the X-ray diffraction pattern of 3.66 Å is intermediate between that of the tetragonal $SrCuO_2$ (3.4 Å) and that of a classical stoichiometric perovskite (3.8–3.9 Å).

The EM study confirms that in a large part of the crystals the "$2a_p\sqrt{2} \times 2a_p\sqrt{2}$" superstructure, parallel to the plane of the substrate, is well established. Similar "$2a_p\sqrt{2} \times 2a_p\sqrt{2}$" superstructures have previously been observed for $La_{5.4}Sr_{2.6}Cu_8O_{20}$ (4) and $YBa_2Cu_3O_{6.15}$ (5). However, in the present cuprate, a very different contrast (Fig. 2) is observed in the HREM images, suggesting that this new phase exhibits an original structure. In [001] images of the thinnest parts of the film, one indeed observes two bright dots spaced by about 3.85 Å along the $[100]_p$ direction; they alternate along that direction with two smaller spots. On the other hand, along the $[010]_p$ direction, every bright dot alternates with three small white spots. In the thicker parts of the film, the main characteristic of the contrast, i.e., the arrangement of two adjacent 3.8 Å-spaced bright dots in an array of gray dots, is retained (Fig. 3). Assuming that these dots are correlated to the positions of strontium and samarium atoms, respectively, a structural model (Fig. 4a) can be proposed for the cationic framework which involves an ordered distribution of Sr and Sm, characterized by two kinds of mixed rows according to the following sequences:

$[Sm–Sm–Sr–Sr]_\infty$ along $[100]_p$,
$[Sm–Sr–Sr–Sr]_\infty$ along $[010]_p$.

In fact the entire cationic array can be described by the stacking along $[100]_p$ of identical $[Sm–Sr–Sr–Sr]_\infty$ rows; two successive double rows are shifted by $2b_p$ with respect to each other, leading to the stacking sequence $(Sm–Sm–Sr–Sr)_\infty$. In addition to the $[Sm–Sm–Sr–Sr]_\infty$ rows parallel to $[100]_p$, one observes pure $[Sr]_\infty$ rows. Note that this cationic distribution, which is in perfect agreement with the film composition deduced from the EDX analysis, does not imply a tetragonal symmetry in spite of the similarity of the two "$2a_p\sqrt{2}$" parameters. To confirm the ordered distribution of Sm and Sr in the framework, focus series of simulated images have been calculated for different crystal thicknesses (t) (t ranging

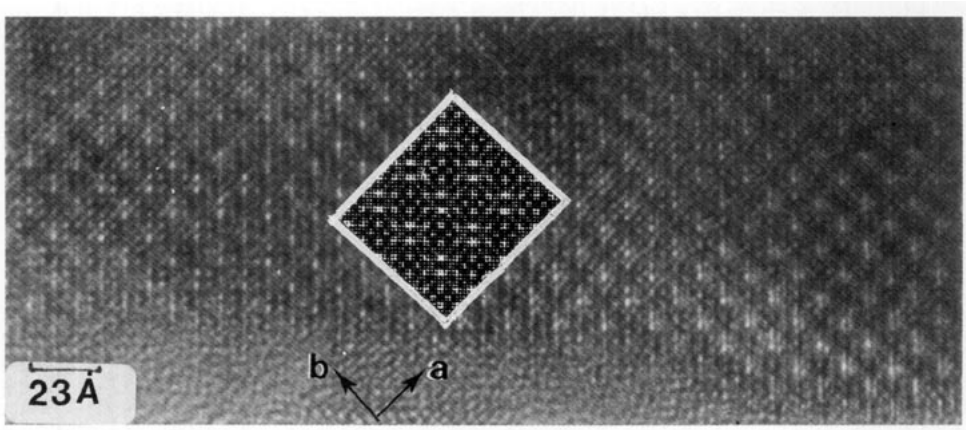

FIG. 2. [001] image of a thin edge of the film; one of the main characteristics of the contrast is the existence of two very bright dots spaced by 3.8 Å when the cation positions are highlighted; they were correlated to the samarium positions. An enlarged simulated image, calculated on the bases of the ideal model in Fig. 4d is shown in insert.

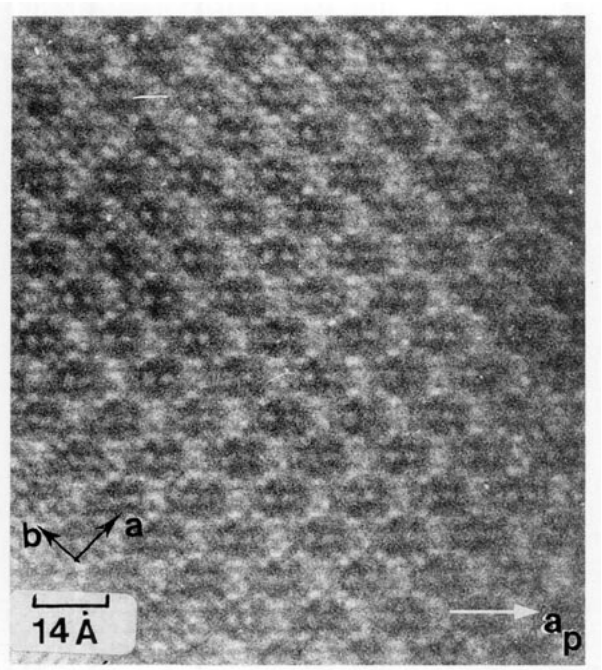

FIG. 3. [001] image recorded in the thicker part of the film: the main characters of the contrast are retained.

from 3 to 9 nm). Starting from the assumed theoretical positional parameters that implies a monoclinic symmetry ($P2/m$ space group, according to the conditions of reflection); the images have been initially calculated with a statistical distribution of the oxygens, according to the infinite layer structure (6, 7) in which each $[CuO_2]_\infty$ layer parallel to the substrate consists of corner-sharing CuO_4 groups. One observes that, for the focus values where the cation positions are highlighted, the two samarium positions appear as very bright dots, compared to the strontium ones. An example is shown in Fig. 4b for $t \sim 5$ nm and $\Delta f \sim 0$. This first series allows to confirm our hypothesis of correlation and of ordering of the Sm/Sr atoms. The next point is to propose a distribution for the anionic framework.

Starting from the infinite layer $SrCuO_2$ structure (6, 7), one can easily propose a distribution of the oxygen atoms in the $(001)_p$ layer. For this purpose, one has to take into consideration that Sm will introduce excess oxygen with respect to $SrCuO_2$, because of its higher valence as compared to Sr. Thus, a model can be proposed: considering that samarium ions form pairs, they may be located in the sites (labeled A) of six-sided tunnels built up from two CuO_5 pyramids and four CuO_4 square planar groups (Fig. 4c). In this arrangement, the strontium atoms, in the sites labeled A', exhibit either a pseudo-cubic eightfold coordination similar to that observed in $SrCuO_2$, or a ninefold coordination. The structure of this new phase (Fig. 4d) is deduced from the $SrCuO_2$ structure, by replacing one $[CuO_2]_\infty$ row of CuO_4 group out of two by one $[Cu_4O_9]_\infty$ row built up from strings of four polyhedra (two CuO_4 square groups + two CuO_5) groups. The simulated images, calculated from the ideal positional parameters of model 3d, do not exhibit drastic differences with those of the first series; as an example, an enlarged calculated image is shown in insert in Fig. 2, where the two bright dots and six gray dots correlated to Sm and Sr positions, respectively, are clearly observed. It should be noted that it is only an idealized model. Images recorded in the thicker parts of the film (Fig. 3) show that, in fact, the framework is slightly distorted. Such a distortion would

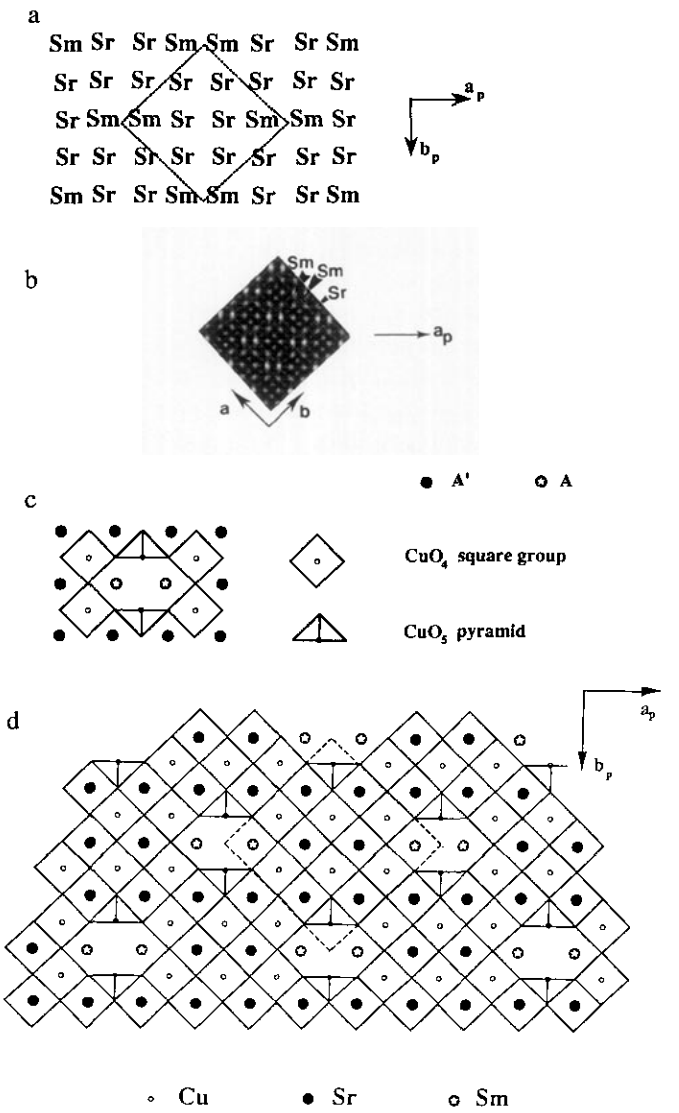

FIG. 4. Structural model proposed for $Sm_2Sr_6Cu_8O_{17}$. (a) Distribution of Sr and Sm atoms in the matrix. (b) Simulated [001] image calculated on the bases of such a cationic framework. (c) Formation of a six-sided tunnel through the presence of additional oxygens in the infinite layer structure. (d) Idealized model viewed along [001]; the supercell is drawn with dotted lines.

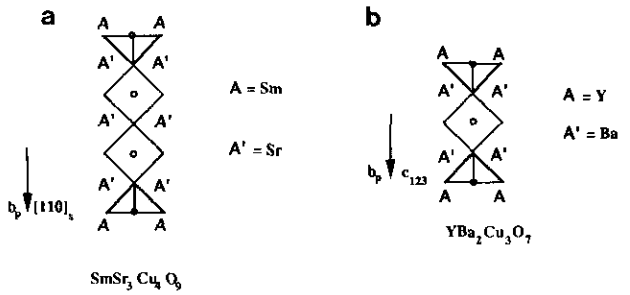

FIG. 5. (a) Idealized drawing of the $SmSr_3Cu_4O_9$ chains, built up from two CuO_5 pyramids and two CuO_4 square groups compared to the "123" structure (b).

be induced both by the ordering of Sm and Sr atoms and also by the ordering of oxygen atoms and vacancies. The formation of six-sided tunnels in which two rare earth or strontium atoms are located would in particular involve a framework distortion as previously shown in other oxides where similar configurations are observed: $La_4BaCu_5O_{13+\delta}$ (14) or $Ln_{2-x}Sr_{1+x}Cu_2O_{6-y}$ (15–17) with Ln = Sm, Nd, or La.

The structure can also be viewed as the intergrowth of two kinds of chains, $[CuO_2]_\infty$ and $[Cu_4O_9]_\infty$ running along $[010]_p$ with two successive $[Cu_4O_9]_\infty$ chains being shifted by $2b_p$ with respect to each other. Then the entire structure can be represented by the formulation $[Sr_3Sm]_2[Cu_4O_8][Cu_4O_9]$, i.e., $Sm_2Sr_6Cu_8O_{17}$. Note that this assumed composition is in perfect agreement with the cationic ratio (EDX analysis) and leads, for Cu(II), rigorously to the "O_{17}" content.

This structural model, which implies introduction of some oxygen atoms between the $(001)_p$ layers in an ordered way, is also supported by the larger value of the c parameter (3.66 Å instead of 3.4 Å), as compared to Sr CuO_2. Moreover it suggests that, depending on the experimental conditions (especially the oxygen pressure), additional oxygen can be intercalated in the structure between the (001) layers, leading to the possible formulation $Sm_2Sr_6Cu_8O_{17+\delta}$ characterized by the mixed valence Cu(II)–Cu(III). This viewpoint is strongly supported by conductivity measurements, the highest conductivity being obtained for this composition, after oxygenation (1).

Considering the $[Cu_4O_9]_\infty$ chains, clear relationships with the "123" structure of $YBa_2Cu_3O_7$ can be observed. The assemblage of such identical chains leads indeed to the theoretical oxygen-deficient perovskite "$SmSr_3Cu_4O_9$" (Fig. 5a) whose structure is deduced from the "123" (Fig. 5b) by introducing an additional $[SrCuO_2]_\infty$ layer between the pyramidal copper plane. Though it could not be prepared as a bulk compound, such a phase $(A,A')_4Cu_4O_9$ was observed as extended defects in thin films (8) and in textured ceramics (9, 10).

From this analysis, it appears that it should be possible to stabilize new intergrowths of the $SrCuO_2$ and $SmSr_3Cu_4O_9$ type structures, with the generic formulation $[A'_4Cu_4O_8]m[AA'_3Cu_4O_9]n$. The oxide $Sm_2Sr_6Cu_8O_{17}$ represents the members $m = n = 1$ of the series, in which the $SrCuO_2$ type and $SmSr_3Cu_4O_9$ type layers are one CuO_4 (or one CuO_5) group wide and where samarium atoms occupy entirely the A sites and partly the A' sites.

Extended Defects: the $Sm_2Sr_2Cu_4O_9$ and $(SmSr_3Cu_4O_9)(SrCuO_2)n$ Members

Besides the major structure described above, extended defects are systematically observed for the Sr/Sm = 3 ratio. This is illustrated in Fig. 6 where three kinds of defects are observed.

In the area labeled ① the bright and small dots are distributed in a different way and the contrast evolves from the top to the bottom parts of the domain. In the top part (curved arrow), one observes double rows of staggered white dots running along the $[110]_p$ direction, separated by two rows of gray spots, leading to a new "$a_p\sqrt{2} \times 2a_p\sqrt{2}$" periodicity in the $(001)_p$ plane of the substrate. This new local superstructure can be interpreted on the basis of a different cationic distribution of Sr and Sm, corresponding to the Sm/Sr ratio equal to 1. The double rows of staggered white dots correspond to Sm, whereas the double rows of gray spots correspond to Sr. Thus the cationic array can be described by the sequences [Sm–Sm–Sr–Sr]$_\infty$ along both directions, $[100]_p$ and $[010]_p$. Then considering that the Sm ions consist of pairs located in similar six-sided tunnels, one obtains the structural model depicted in Fig. 7a. Similar to $Sm_2Sr_6Cu_8O_{17}$, the structure consists of $[Cu_4O_9]_\infty$ rows built up of strings of

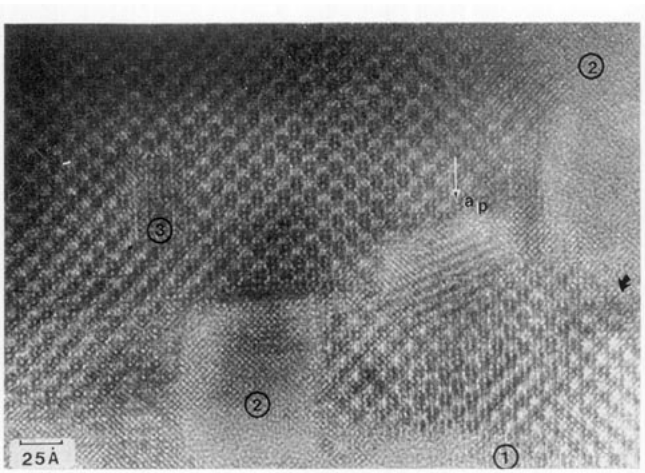

FIG. 6. Enlarged [001] image exhibiting three types of extended domains, in the $2a_p\sqrt{2} \times 2a_p\sqrt{2}$ matrix. The local periodicities are domain ①; $a_p\sqrt{2} \times 2a_p\sqrt{2}$; domain ②, $a_p \times a_p$; and domain ③, $a_p \times na_p$.

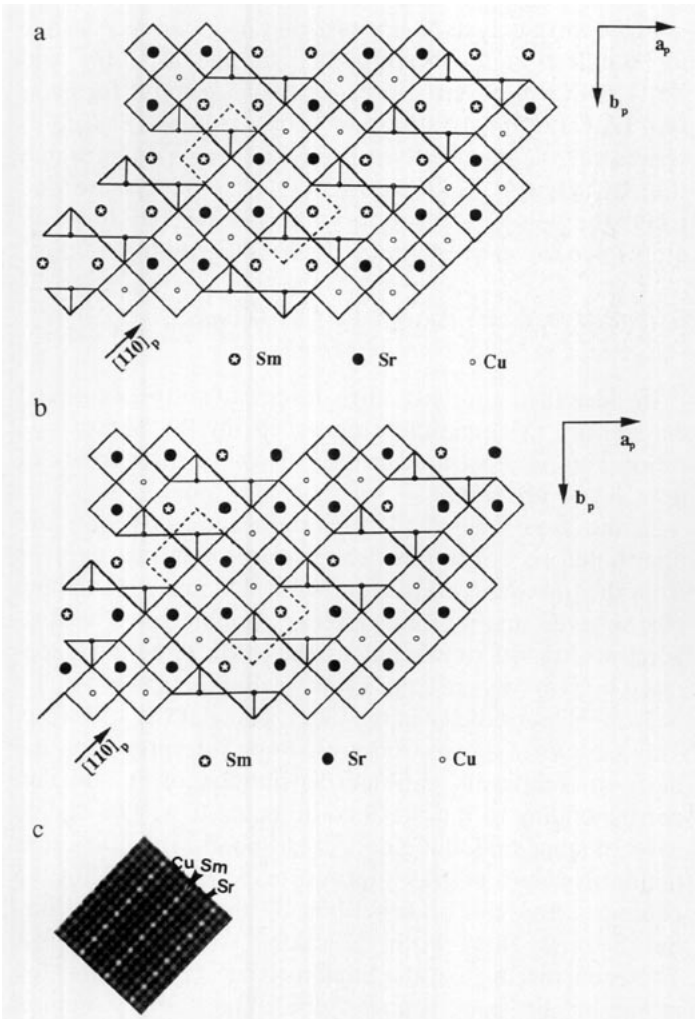

FIG. 7. Idealized models proposed for the $a_p\sqrt{2} \times 2a_p\sqrt{2}$ supercell: (a) $Sm_2Sr_2Cu_4O_9$; (b) $SmSr_3Cu_4O_{9-\delta}$; and (c) calculated image corresponding to such a distribution (to be compared with the bottom part of area ① in Fig. 6).

two CuO_5 pyramids and two CuO_4 square planar groups running along $[010]_p$, but the $[CuO_2]_\infty$ rows have now disappeared. In this structure, the successive $[Cu_4O_9]_\infty$ rows are shifted by a_p with respect to each other. As a result, the chemical composition corresponding to this framework can be formulated as $Sm_2Sr_2Cu_4O_9$. Note that this phase derives from the hypothetical structure $SmSr_3Cu_4O_9$ by a translation of one $[Cu_4O_9]_\infty$ row out of two along b_p, resulting in a different Sm/Sr ratio that induces the formation of six-sided tunnels. Such a model implies a valence (II) for copper, but a local variation of the Sm/Sr ratio around 1, i.e., involving an excess of Sr which are located on the Sm sites, is also possible so that it could induce the Cu(II)–Cu(III) mixed valence. The substitution of Sr for Sm sometimes occurs in an ordered way as observed in the bottom part of area ①. One observes then that double rows of staggered white dots are replaced by the new sequence: a single row where one bright dot alternates with one gray dot (involving an $a_p\sqrt{2}$ periodicity) and three rows of gray dots, involving a $2a_p\sqrt{2}$ periodicity in the perpendicular direction. On the basis of the previous correlation, the contrast can be interpreted as an ordered substitution of one Sm atom out of two by Sr in the six-sided tunnels, as shown in the structural model of Fig. 7b. Images (Fig. 7c) have been calculated for this ideal model (Fig. 7b); they confirm that the experimental contrast is consistent with such a distribution. The brightest dots, correlated to the samarium positions, are separated by gray dots associated with the copper ones; the three rows of gray dots are correlated to the strontium and ccopper atoms. Such a substitution involves a Sm/Sr ratio which matches exactly with that of the nominal composition, i.e., $SmSr_3Cu_4O_9$. Thus, for Sm/Sr ratio of 0.75, two orthorhombic perovskites are observed, with $2a_p\sqrt{2} \times 2a_p\sqrt{2} \times a_p$ and $a_p\sqrt{2} \times 2a_p\sqrt{2} \times a_p$ superstructures, respectively. The first one $Sm_2Sr_6Cu_8O_{17}$ is stabilized

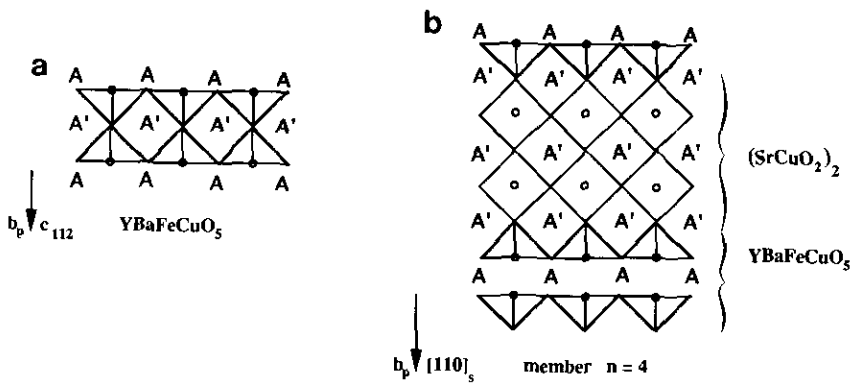

FIG. 8. Idealized models of (a) the $YBaFeCuO_5$-type structure and (b) the intergrowth of $(SmSrCu_2O_5)(SrCuO_2)_2$ structure built up from "$SmSr_3Cu_4O_9$" chains (Fig. 5a).

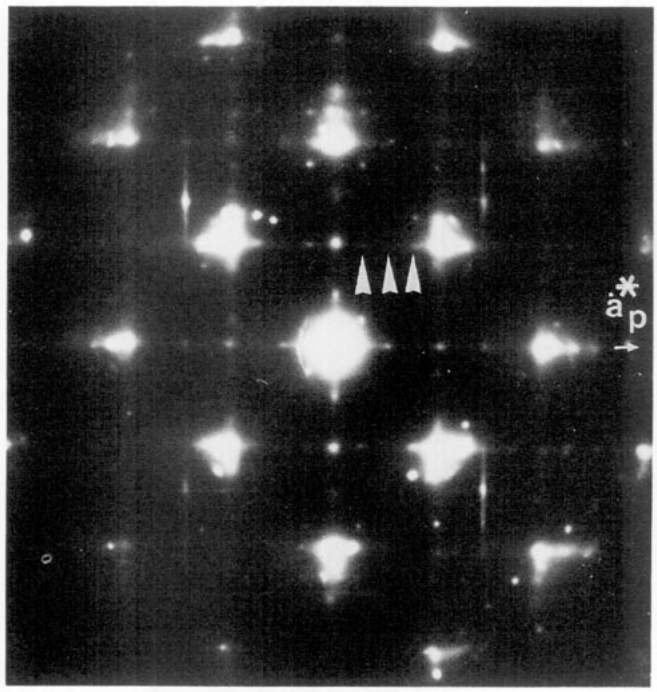

FIG. 9. [001] ED pattern exhibiting streaks along a^*. The maxima are marked by white arrows.

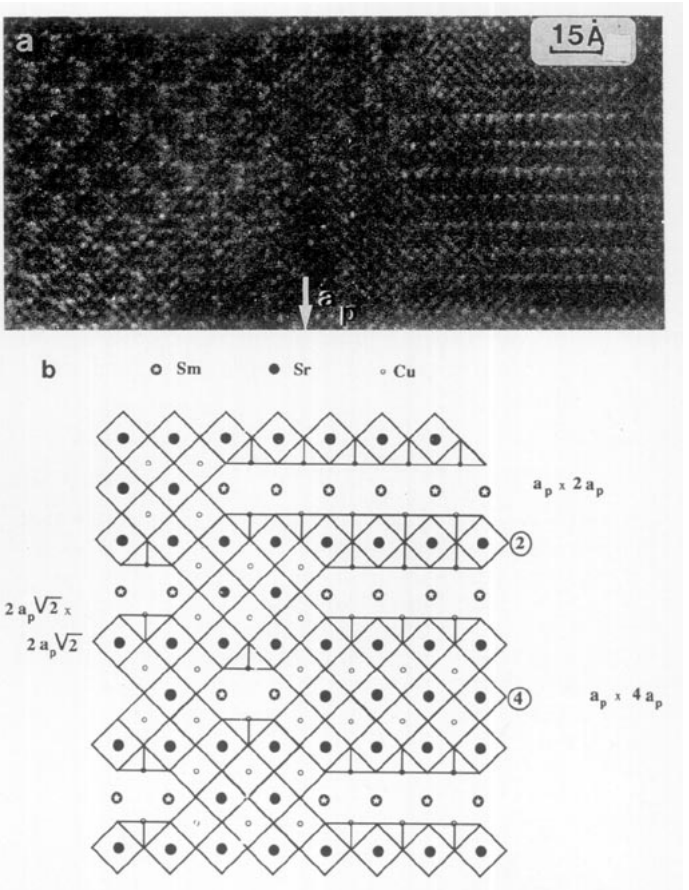

FIG. 10. (a) [001] image of a defective zone where an "$a_p \times na_p$" domain is coherently connected to a $2a_p\sqrt{2} \times 2a_p\sqrt{2}$ domain; (b) idealized model of the connection ($n = 2$ and $n = 4$ are taken as examples).

throughout the whole matrix of the thin films whereas the second $SmSr_3Cu_4O_9$ ($a_p\sqrt{2} \times 2a_p\sqrt{2}$) is less stable and only observed in the form of small domains; this could be due to the oxygen content which would involve a rather high Cu(III) content.

The areas labeled ② correspond to the well-known contrast of the $SrCuO_2$-type structure "$a_p \times a_p$." They are often associated with small areas where the contrast is highly disturbed.

In the area labeled ③ "$a_p \times na_p$" superstructures are observed with $n = 2$ and 4. The $n = 2$ member can be interpreted as the phasoid $SmSrCu_2O_5$ which would have the $YBaFeCuO_5$ structure (11), built up from layers of corner-sharing CuO_5 pyramids (Fig. 8a). The $n = 4$ member can be interpreted as the phasoid $SmSr_3Cu_4O_9$ built up from "$SmSr_3Cu_4O_9$" chains (Fig. 5a) and that corresponds to the intergrowth of one $YBaFeCuO_5$-type layer with two $SrCuO_2$-type layers (see Fig. 10b). In general, such intergrowths with the generic formulation $(SmSrCu_2O_5).(SrCuO_{2n-2})$ can be observed in different crystals. Such defects are sometimes observed in more extended areas; in which case, the SAED patterns exhibit diffuse streaks, but with maxima for $(0\ \frac{1}{4}\ 0) : (0\ \frac{1}{2}\ 0) : (0\ \frac{3}{4}\ 0)$ (Fig. 9, white arrowheads).

The images of Fig. 6 (area ③) and Fig. 10a show that the systems of white dots of the two structures "$2a_p\sqrt{2} \times 2a_p\sqrt{2}$" and "$a_p \times na_p$" are aligned without any significant distortion. This suggests that the ordering of the Sm and Sr cations is coherent from one structure to the other. As an example, a model of such a transition between the $Sm_2Sr_6Cu_8O_{17}$ ("$2a_p\sqrt{2} \times 2a_p\sqrt{2}$") structure and the $SmSr_3Cu_4O_9$ ("$a_p \times 4a_p$") structure is displayed in Fig. 10b.

Besides the above extended defects, isolated defects corresponding to the absence of a copper layer are sometimes observed in the small areas where the $SrCuO_2$-type structure is established. The double $[AO]_\infty$ layer which results from this mechanism is perpendicular to the substrate.

CONCLUDING REMARKS

The synthesis of a new ordered phase $Sm_2Sr_6Cu_8O_{17+\delta}$ in the Sm–Sr–Cu–O system further demonstrates the capacity of the laser ablation method in stabilizing new metastable phases in the form of thin films. This is in agreement with our previous results of the Y–Ba–Cu–O (12), La–Ba–Cu–O (13), and La–Sr–Cu–O (2) systems

that have allowed several new perovskites to be obtained. In the Sm–Sr–Cu–O system, with Sm/Sr = 0.75, three different ordered perovskites have been characterized. The first one ($2a_p\sqrt{2} \times 2a_p\sqrt{2}$) is stable and established throughout the whole film, whereas the two others, $a_p\sqrt{2} \times 2a_p\sqrt{2}$ and $a_p \times 4a_p$, arise in the form of extended defects.

It appears quite likely that other ordered structures can be stabilized in the Sm–Sr–Cu–O system by varying the Sm/Sr ratio and the deposition conditions. The HREM study of the various thin films of the system "$Sm_{1-x}Sr_xCuO_{2.5+0.5x+\delta}$" corresponding to different nonimal x values is in progress.

ACKNOWLEDGMENTS

This work was carried out as part of a joint contract between IBM, CNRS, and Région de Basse-Normandie.

REFERENCES

1. A. Gupta, B. Mercey, M. Hervieu, and B. Raveau, *Chem. Mater.* **6** and **7,** 1011 (1994).
2. M. Y. Chern, A. Gupta, and B. W. Hussey, *Appl. Phys. Lett.* **60,** 3046 (1992).
3. M. Y. Chern, A. Gupta, B. W. Hussey, and T. M. Shaw, *J. Vac. Sci. Technol. A* **11** 637 (1993).
4. (a) L. Er-Rakho, C. Michel, and B. Raveau, *J. Solid State Chem.* **73,** 514 (1988); (b) C. Michel, L. Er-Rakho, and B. Raveau, *J. Phys. Chem. Solids* **49,** 451 (1988).
5. T. Krekels, T. S. Shi, J. Reyes-Gasga, G. Van Tendeloo, J. Van Landuyt, and S. Amelinckx, *Physica C* **167,** 677 (1990).
6. T. Siegrist, S. M. Zahurak, D. W. Murphy, and R. S. Roth, *Nature* **334,** 231 (1988).
7. N. Sugri, M. Ichikawa, K. Hayashi, K. Kubo, K. Yamamoto, and H. Yamauchi, *Physica C* **213,** 345 (1993).
8. R. Ramesh, D. M. Hwang, J. Venkatesan, T. S. Ravi, L. Nazar, A. Inam, X. D. Xu, B. Dutta, G. Thomas, A. F. Marshall, and T. H. Geballe, *Science* **247,** 57 (1990).
9. A. Ourmazd, J. A. Rentschler, J. C. H. Spence, M. O'Keefe, R. J. Graham, D. W. Johnson, Jr., and W. W. Rhodes, *Nature* **327,** 308 (1987).
10. B. Domengès, M. Hervieu, B. Raveau, J. Karpinski, E. Kaldis, and S. Rusiechi, *J. Solid State Chem.* **93,** 316 (1991).
11. L. Er-Rakho, C. Michel, Ph. Lacorre, and B. Raveau, *J. Solid State Chem.* **73,** 53 (1988).
12. J. F. Hamet, B. Blanc-Guilhon, A. Taffin, B. Mercey, M. Hervieu, and B. Raveau, *Physica C* **214,** 55 (1993).
13. R. Desfeux, J. F. Hamet, B. Mercey, Ch. Simon, M. Hervieu, and B. Raveau, *Physica C* **221**(1 and 2), 205 (1994).
14. C. Michel, L. Er-Rakho, M. Hervieu, J. Pannetier, and B. Raveau, *J. Solid State Chem.* **68,** 143 (1987).
15. J. R. Grasmeder and M. T. Weller, *J. Solid State Chem.* **85,** 88 (1990).
16. V. Caignaert, R. Retoux, C. Michel, M. Hervieu, and B. Raveau, *Physica C* **167,** 483 (1990).
17. M. Hervieu, V. Caignaert, C. Michel, R. Retoux, and B. Raveau, *Microsc. Microanal. Microstruct.* **1,** 2(1990).